

Characterization of Niobia-alumina Deposited by the Sol-gel Process on Carbon Steel

Solange Francisco do Nascimento^{a*}, Antônio José do Nascimento Dias^b, Guilherme Magliano da Silva^a, Hugo de Souza Caldeira^a, Luís Henrique Leme Louro^c, Wilma de Araújo Gonzalez^c

^aUniversidade do Estado do Rio de Janeiro, Instituto Politécnico, R. Bonfim, 25, 28.625-570, Nova Friburgo, RJ, Brasil

^bInstituto Nacional de Tecnologia, Av. Venezuela, 82, 20.081-312, Rio de Janeiro, RJ, Brasil

^cInstituto Militar de Engenharia, Praça General Tibúrcio, 80, 22.290-270, Rio de Janeiro, RJ, Brasil

Received: May 26, 2017; Revised: January 27, 2018; Accepted: March 06, 2018

The precursor sols of Al_2O_3 and mixed $\text{Nb}_x\text{O}_y/\text{Al}_2\text{O}_3$ oxides were synthesized by the sol-gel process using acetylacetone to control the reaction kinetics of the organometallic oxides in the mixture. The layers of the precursor sols of Al_2O_3 and $\text{Nb}_x\text{O}_y/\text{Al}_2\text{O}_3$ were deposited on AISI steel 1020 by manual immersion (dip coating). The lyophilized sols were characterized by X-ray diffraction, thermal analysis and scanning electron microscopy with EDXS before the recoating process. The influence of the ceramic coating of corrosive processes of AISI steel 1020 were investigated by electrochemical measurements. The only identified phase was poorly crystallized boehmite with homogeneous mixture of Al, Nb, O and C ions in mixed $\text{Nb}_x\text{O}_y/\text{Al}_2\text{O}_3$ oxides. The ceramic layers deposited appeared to have physical and chemical homogeneity and the steel samples with these deposits had lower corrosion potential. However, the precursor sol Al_2O_3 showed better steel corrosion protection with lower current density, and more corrosive potential.

Keywords: Corrosion, Sol-gel, Niobia, Alumina.

1. Introduction

Sol-gel is a wet synthesis method that is suitable to produce powders, fibers, thin films and monoliths. Ceramic layers can be deposited by sol-gel on metal and glass substrates^{1,2,3}. The precursors of ceramics are a colloidal dispersion named⁴. This dispersion can be applied on a substrate by spin coating, dip coating or spray coating^{1,5}. They are simple techniques that do not use expensive equipment, as is the case of chemical vapor deposition (CVD) and physical vapor deposition (PVD)⁶. Moreover, large substrates with or without complex shape can be easily coated with ceramic layers or even hybrid organic/inorganic layers^{6,7,8,9}. This process does not present the common problems related to dry deposition, sputtering or vapor deposition. Consequently, this method is especially attractive to produce protective layers. Additionally, the sol-gel technique allows the synthesis/processing of deposits with multicomponents and multilayers^{7,10}. The materials are mixed at the molecular level, at low temperatures. The physical characteristics are tailored by adjusting the viscosity, surface tension and/or concentration of the polymeric solution⁷.

The properties of sol-gel deposited layers on metals and glass have been investigated taking into account diverse aspects, as reported by¹¹. These layers can be superhydrophobic, to form self-cleaning surfaces¹²; photocatalytic and superhydrophilic, to promote self-cleaning and anti-fogging¹³; or anti-reflective at visible wavelength for automotive glass, solar panels, glass lenses, window panes, etc.¹⁴. Besides these, many other properties are possible, such as tribological properties

for microelectronic components, and biocompatibility and bioactivity to stimulate tissue growth, among others^{14,15,16,17}.

Anticorrosive properties of sol-gel coating have been studied in oxide and non-oxide ceramics, with single or multiple components^{5,9,18,19,20}. Generally, ceramics are more resistant to corrosion than metals. They also exhibit higher hardness and wear resistance, besides dielectric properties. These characteristics make ceramics attractive materials to coat metals to improve their resistance to corrosion²⁰. The sol-gel process produces protective layers of ceramics and hybrids (inorganic-organic) on metallic substrates without affecting the microstructure or mechanical properties because it can be carried out in a low temperature range¹⁸.

Several studies have reported the protection of metals produced by sol-gel using pure oxides and mixtures of oxides, chiefly based on TiO_2 , Al_2O_3 , SiO_2 , ZrO , etc.^{5,6,20,21,22}. However, studies of the use of Nb_2O_5 in compositions containing single or multiple components are scarce.

Metallic niobium and its alloys are employed in the aerospace and chemical industries and nuclear plants. It is a refractory metal with melting point of 2,468 °C. Another important use is as alloying element of stainless steels and non-ferrous alloys. Niobium is very resistant to high temperature corrosion. Moreover, it is resistant to aggressive media such as hydrochloric, sulfuric, and organic acids at high pH. Besides these aspects, it resists liquid metals well. A passive film forms very quickly when in contact with air or water that causes higher

*e-mail: kucaime@yahoo.com.br

resistance than that of stainless steel. This layer forms spontaneously, is very adherent and remains passive in oxidant or reductive environments due to the capacity to change its oxidation numbers from +1 to +5. The formed film may include Nb in various oxidation states - NbO, NbO₂ and Nb₂O₅, or a mixture thereof. NbO and NbO₂ are unstable in aqueous media since they both react in water. However, NbO₂ releases hydrogen, becoming oxidized and forming Nb₂O₅ ($2 \text{NbO}_2 + \text{H}_2\text{O} \rightarrow \text{Nb}_2\text{O}_5 + \text{H}_2$). Nb₂O₅ is the most thermodynamically stable phase. The compounds with oxidation number lower than +5 are formed in reducing environments and are less stable²³.

On the other hand, sol-gel alumina coating on diverse metallic substrates has been found efficient against corrosion^{24,25,26,27}. In this sense, in the present study we combined the Al₂O₃ and Nb_xO_y-Al₂O₃ layers. Each material was synthesized by the sol-gel route and deposited on UNS G10200 from alcokside. The characterization of lyophilized sols, precursors of Al₂O₃ and Nb_xO_y-Al₂O₃, were performed by thermal analysis, X-ray diffraction, scanning electronic microscopy and dispersive X-ray energy. The corrosion behavior of the deposited layers was evaluated by polarization curves in 3.5% NaCl at 25 °C.

2. Materials and Methods

2.1 Synthesis of Al₂O₃ and Nb_xO_y/Al₂O₃ sol precursor

All solvents and reagents used in the experiments were of analytical grade (supplied by Merck). The alumina sol was prepared in a dry chamber (Plas Labs Inc. model 850-NB/110), by mixing isopropoxyde of aluminum with Milli-Q water at a molar ratio of 1:100 (alkoxide:water) under agitation and reflux. The temperature was in the range 80 to 90 °C to allow complete hydrolysis of alkoxide. After one hour of mixing, HNO₃ (1.5 M) was added to maintain the suspension's pH below 4. This pH facilitates the peptization of particles. The obtained sol was kept under agitation, heated from 80 to 90°C along with reflux for 18 hours after peptization. Subsequently, the sol was immediately frozen and then lyophilized. The sol was the precursor of the mixed Nb_xO_y/Al₂O₃ oxides, as described before.

During the peptization of Al₂O₃ sol, a solution of nitric acid in alcohol (1.0 M) was added. One hour later, niobium pentaoxide and anhydrous isopropyl alcohol were added in bohemitic sol. In this case, the temperature (80 - 90 °C), agitation and reflux were maintained for 18 hours, to the end of peptization. The sol, which was transparent, was frozen and lyophilized. The content of Nb_xO_y in Nb_xO_y-Al₂O₃ was 5%. To control the hydrolysis/condensation of niobium alkoxide, acetylacetone at 2:1 molar ratio (niobium pentaoxide: acetylacetone) was used as complexing agent of alkoxide.

2.2 Deposition and heat treatment

The layer deposition of Al₂O₃ and Nb_xO_y/Al₂O₃ sol was executed manually, without control of withdrawal rates and dwell times. 1.00 g mass of lyophilized Al₂O₃ or Nb_xO_y/Al₂O₃ sol was re-dispersed in 25 mL of Milli-Q water under mechanical stirring at room temperature for 30 min.

Samples of UNS G10200 steel were abraded with emery paper up to #600. After this, they were washed with water and dried with hot air. Isopropyl alcohol was used to clean the surfaces before immersion in the electrolyte. The samples were immersed immediately after the surface preparation. Afterward, the samples were dried for 30 min at room temperature and subsequently heat treated at the 300°C in an oven. This procedure was repeated until obtaining Al₂O₃ and Nb_xO_y/Al₂O₃ layers. A sample of the same steel, but without coating, was used to compare the effect of the layers in corrosion tests.

2.3 X-ray diffraction and scanning electronic microscopy

X-ray diffraction analysis was performed on the lyophilized precursor sol of Al₂O₃ and Nb_xO_y/Al₂O₃. A Philips X-Pert Plus diffractometer with Cu K α radiation was used. The lyophilized powder was also analyzed by scanning electron microscopy, with a FEI Quanta FEG 450 microscope attached to an energy dispersive X-ray spectrometer (EDXS). To improve the quality of images, the samples were coated with platinum to avoid the accumulation of incident electrons.

2.4 Thermal analysis

Thermal analysis was performed on the lyophilized precursor sol of Al₂O₃ and Nb_xO_y/Al₂O₃ using a SDT Q600 V3 4 Build 41 Instruments, DSC - TGA Standard Module. The samples were heated under oxygen flow of 100 mL.min⁻¹ and heating rate of 5 °C.min⁻¹ for the three tests: thermogravimetric analysis (TGA), the differential thermal analysis (DTA) and differential scanning calorimetry (DSC).

2.5 Electrodynamic measures

Potentiometric assays were performed on samples with precursor sol coatings of Al₂O₃ and Nb_xO_y/Al₂O₃. An Ametek VersaSTAT 3 potentiostat, controlled by the VersaStudio software, was used in this experiment. A three electrode electrochemical cell was used, the sample being the working electrode, a platinum filament as against electrode and a saturated calomel electrode (ECS) as reference electrode, with an area of exposure to the electrolyte of 1 cm². The polarization was performed from - 500 mV in relation to the open circuit potential at 1.6 V of the reference electrode, at a scanning speed of 1 mV.s⁻¹, at room temperature. To study the effects of corrosion protection of metallic layers deposited on the substrate, potentiometric analyses were performed on low carbon steel samples without coating for comparison purposes.

In these assays, the faces of all samples were sanded with sandpaper #100, so that the metal surface was completely exposed, free of coatings or oxidation products, and in contact with a copper conductor wire. The other side, coated or uncoated, was placed in contact with an aqueous solution of 3.5% NaCl.

3. Results and Discussion

3.1 X-ray diffraction

Fig. 1 shows the X-ray diffractograms of the lyophilized samples. It can be observed that for both samples, the X-ray diffraction peaks are not well defined, indicating a poorly crystallized structure. Thus, the peaks correspond to a gelatinous or poorly crystallized boehmite, also known as pseudoboehmite²⁸. No crystalline phases of niobium compounds which diffraction peaks at 2θ in $22,0^\circ$ (80%), $28,1^\circ$ (100%) and $36,2^\circ$ (80%) don't be observed.

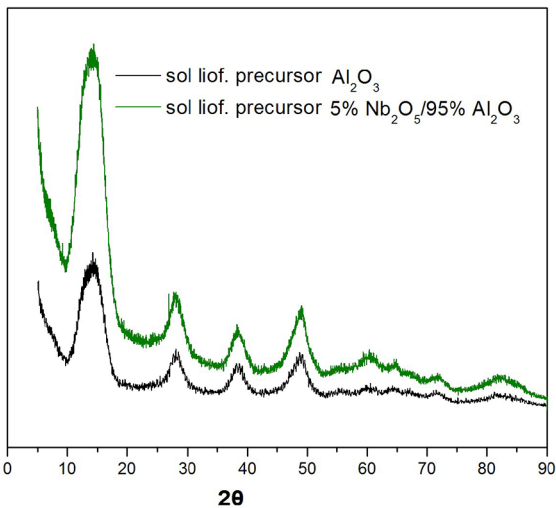


Figure 1. X-ray diffractogram of lyophilized sol. (a) Pure Al_2O_3 and with (b) 5% $\text{Nb}_x\text{O}_y/95\% \text{Al}_2\text{O}_3$

Pseudoboehmite has a disorder in the crystalline structure, also known as a defective or poorly crystallized crystalline structure²⁸. In contrast, the boehmite diffractogram is characterized by intense and acute diffraction with $I(f) = 100$ at $2\theta = 18:23$ and $D020 = 0.611$ nm. Tettenhorst and Hofmann (1980) concluded that no significant difference in the X-ray diffraction of these two types of boehmite lies mainly in variations of sizes of the crystallites. Thus, for pseudoboehmite has X-ray spectra in the enlargement diffractions which are characteristic of well-crystallized boehmite²⁹.

3.2 Thermal analysis

The precursor lyophilized samples of Al_2O_3 and $\text{Nb}_x\text{O}_y/\text{Al}_2\text{O}_3$ mixed oxides, with nominal proportions of 5% and 95%, respectively, were subjected to thermal analysis. The results are shown in Fig. 2. Fig. 2a shows three weight loss steps in the thermal evolution of the lyophilized sol of Al_2O_3 , extending from 28°C to 474°C , with a total mass loss 39.7%. An endothermic peak is observed in the first stage, starting at 28°C and ending at 208°C , according to the differential thermal analysis (Fig. 2a). This indicates that in this step there was weight loss associated with the removal of water molecules adsorbed in the pores of the boehmite, as well as an organic waste release, which is always present in sol-gel synthesis. In this first step, the mass loss was 20.5%. The intermediate mass loss step (from 208°C to 345°C) was small and corresponded to the removal of water molecules. In this region, a discontinuity can be observed at 323°C in the DSC curve (Fig. 2a), indicating the characteristic thermal decomposition of the pseudoboehmite.^{30,31,32} The last weight loss step (from 345°C to 474°C), indicated by an endothermic peak in the DTA and DSC curves (Fig. 2a), results from the dehydroxylation of boehmite, becoming $\gamma\text{-Al}_2\text{O}_3$. The crystallization of this phase continued with the rise in temperature to 705°C , as shown in the DSC curve (Fig. 2a), characterized by an endothermic peak starting at 474°C without loss of mass.

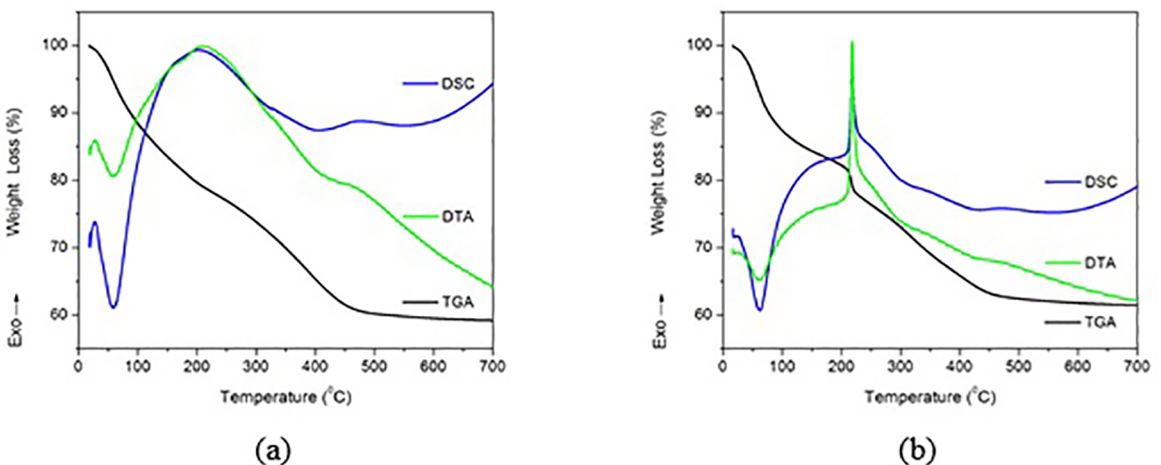


Figure 2. Thermal evolution curves - Thermogravimetric analysis (TGA), differential thermal analysis (DTA) and differential scanning calorimetry (DSC) - lyophilized precursor sol of: (a) Al_2O_3 ; and (b) mixed oxides of $\text{Nb}_x\text{O}_y/\text{Al}_2\text{O}_3$

The thermal stability of the lyophilized precursor sol $\text{Nb}_x\text{O}_y/\text{Al}_2\text{O}_3$, with nominal amounts of 5% and 95% of Nb_xO_y and Al_2O_3 , respectively, was investigated by thermal analysis, whose results are shown in Fig. 2b. Three distinct mass loss stages were observed in the range 28 °C to 474 °C, with a total weight reduction of 37.4%. This value is very close to that of the lyophilized sample of Al_2O_3 described above. The DTA curve shows an endothermic peak (28 °C to 208 °C), which corresponds to the elimination of water adsorbed in the pores of the boehmite and detachment of CO_2 , but with 18.4% mass loss. The presence of the complexing agent forming acetylacetonate Nb (acac), used to control the rate of hydrolysis and condensation of niobium isopropoxide, decreased the amount of water adsorbed on $\text{Nb}_x\text{O}_y/\text{Al}_2\text{O}_3$. The sharp exothermic peak centered around 210 °C appears in the DSC curve, accompanying the abrupt mass loss observed in the TGA curve (Fig. 2b). This energy release corresponds to the decomposition of acac ligands of the Nb complex (acac)_n. This mechanism is called proton-assisted thermolysis, where the surface of the substrate (Al_2O_3 precursor) protonates the ligand, catalyzing the formation of 2,4-pentanedione, which leaves the surface of the lyophilized sol as a gas at low temperature³³.

The characteristic of the abrupt decrease in weight loss, indicating rapid elimination of organic material at a relatively low temperature, was associated by Ahenach et al. (2000) with a very uniform pore structure of the material³³. This structure allows the decomposition of significant quantities of organic compounds in a narrow temperature range. Additionally, this abrupt decrease was also associated with a homogeneous dispersion of particles by Uekawa et al. (2003), when studying the synthesis of niobium oxide nanoparticles at low temperature³⁴.

The final weight loss step ending at 474 °C had characteristics similar to those noted in the thermal studies of the precursor sol Al_2O_3 . This mass loss corresponds to the dehydroxylation of boehmite for nucleation in $\gamma\text{-Al}_2\text{O}_3$, whose crystallization occurs with increasing temperature.

3.3 Scanning electron microscopy

Energy dispersive X-ray spectroscopy (EDXS) were performed on lyophilized samples of 5% Nb_xO_y in 95% Al_2O_3 . This technique was used to identify the chemical elements present in the sample and synthesized, to evaluate their dispersion. Two areas of the $\text{Nb}_x\text{O}_y/\text{Al}_2\text{O}_3$ sample, on the same specimen holder (Fig. 3a) were subjected to microanalysis with magnification of 100 X. The mapping of the identified chemical elements (Al, Nb, C, O and Pt) with 2000 X magnification (Fig. 3b).

The EDXS spectra of the two regions of the $\text{Nb}_x\text{O}_y/\text{Al}_2\text{O}_3$ sample (Fig. 4a and Fig. 4b) enabled identifying

the chemical elements aluminum, niobium, oxygen and carbon. The presence of carbon stems from aluminum isopropoxide agents and niobium pentaethoxide precursors, since the analyzed sample was only lyophilized, without any heat treatment.

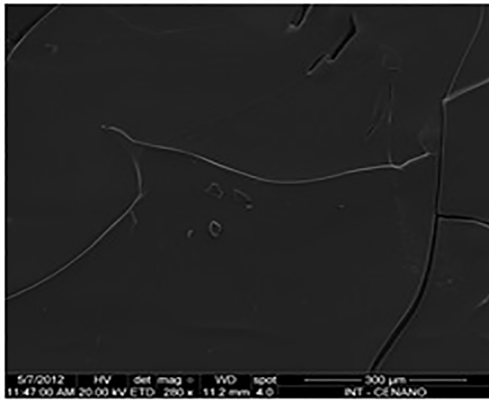
The mapping of the identified chemical elements (Al, Nb, C, O and Pt), of the $\text{Nb}_x\text{O}_y/\text{Al}_2\text{O}_3$ sample are shown in Figures 4. The existence can be seen in areas of uniform distribution of the Nb atom (Nb_xO_y) in relation to the Al atoms (Al_2O_3) of the synthesized powder.

Due to the nanometric nature of the cover it is impossible to any morphological characteristic of the cover. The presence of pseudoboehmite and niobia can be observed by the EDS of powder.

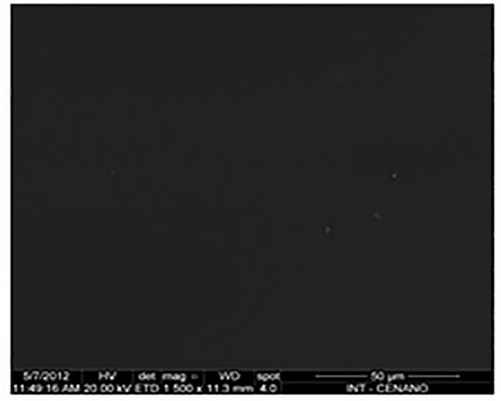
This is a promising method for the synthesis of nanoparticles with high purity and strict control of composition. This facilitates the synthesis of mixed compounds at low temperatures. However, in the case of synthesis of oxide mixtures, the kinetics of chemical reactions of the precursors need to be controlled. The various speeds of hydrolysis and condensation of alkoxide precursors become a problem, since the nucleation and growth of the colloidal particles exhibit different kinetics. Thus, particles can be synthesized with various sizes along with obtaining non-homogeneous distribution of the crystalline phases or the separate precipitation of components¹⁰. However, the use of complexing agents such as acetylacetonate attenuates these effects, by controlling the speed of hydrolysis and condensation of these precursors, allowing obtaining more homogeneous dispersion phase and narrower particle size distribution. Thus, it appears that controlled kinetics of chemical reactions occurred in this study, since the energy dispersive X-ray mapping of aluminum and niobium presents a homogeneous distribution, as shown in Figs 5 and 6. This is due to the use of the complexing agent acetylacetonate. These observations are compatible with the characteristic of abrupt decrease in mass loss observed in the thermal analysis, which were associated with homogeneous dispersion of Nb_2O_5 by Uekawa et al. (2003)³⁴.

3.4 Electrodynamic measures

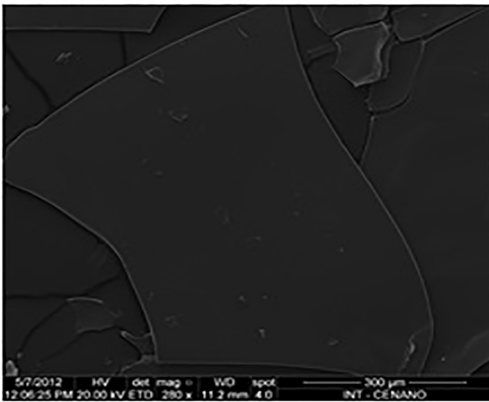
The metal oxide films produced by immersion of sols synthesized by the sol-gel process can generate significant residual stresses that can result in cracks. This occurs because the films are densified by volume reduction due to the capillary pressure generated by evaporation of the solvent and the polycondensation reactions during the heat treatment step of the film on the substrate. Another important aspect to be considered in the coating process is the different coefficients of thermal expansion between the substrate and the deposited film, because this difference generates thermal stress during the heat treatment conducted to diffuse the coating on the substrate and to ensure good adhesion^{35,36}.



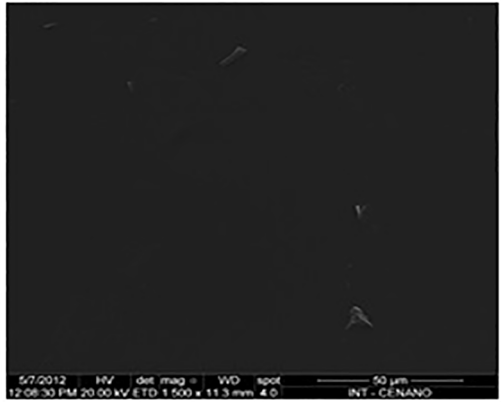
a)



b)

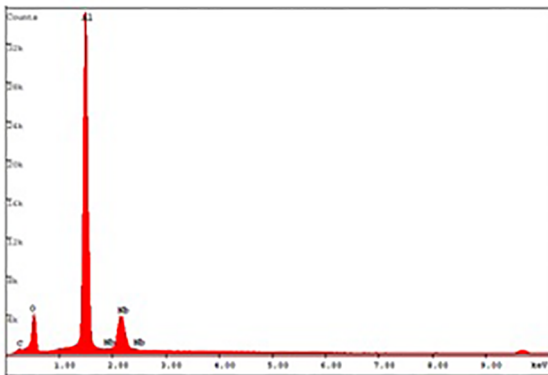


c)

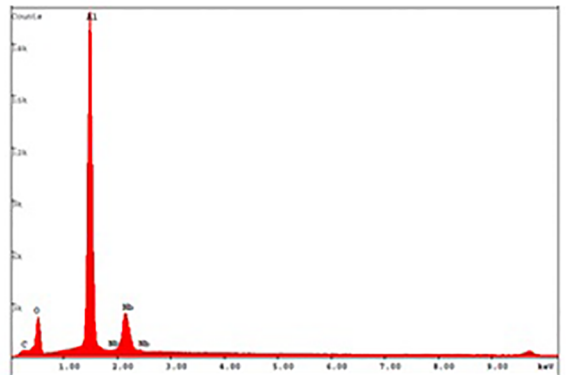


d)

Figure 3. Scanning electron microscopic images of the sample containing 5% Nb_xO_y in 95% Al₂O₃: a) microanalysis of A1 and A2 with 100 X magnification; b) mapping by EDXS 2000 X magnification



a)



b)

Figure 4. Energy dispersive X-ray spectra of the sample of 5% Nb_xO_y in 95% Al₂O₃, Area 1 (a) and Area 2 (b)

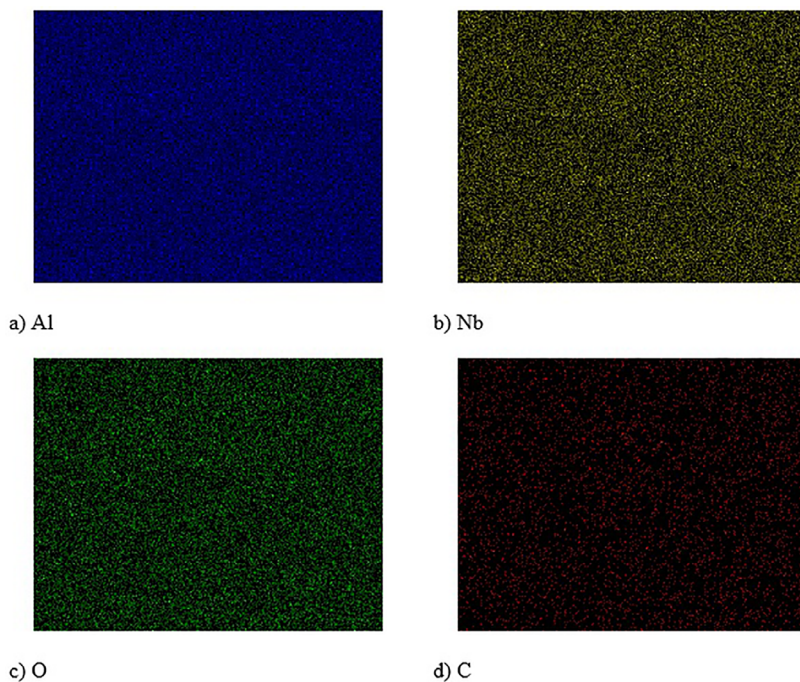


Figure 5. Mapping by EDXS of chemical elements present in the sample of 5% Nb_xO_y in 95% Al_2O_3 : a) aluminum; b) niobium; c) oxygen; d) carbon; and e) platinum

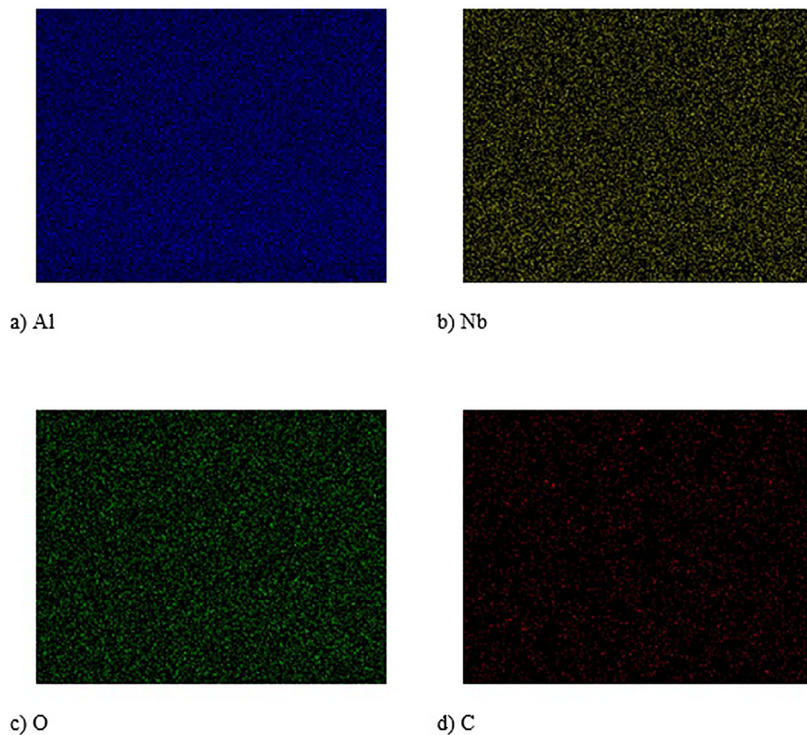


Figure 6. Polarization curves for AISI steel 1020, 3.5% NaCl, at room temperature, coated with mixed oxide precursor sol of Nb_xO_y/Al_2O_3 with nominal values of 5% and 95%, respectively

On the other hand, it is always important to assess the homogeneity of the films on the substrate, not only the homogeneity of the composition of the mixed oxide, as detected by energy dispersive X-ray analysis of the lyophilized powder. To assess the homogeneity of these mixed oxide films, we used potentiodynamic polarization curves, which assess the stability of the film and indirectly indicate a homogeneity of the mixed oxide film. This technique is used to evaluate the surfaces of different materials with respect to corrosive processes. The spontaneous passivating films or those made by other processes should be uniform, dense and free of cracks and have good adhesion to the substrate. These characteristics can be evaluated by polarization curves, as shown in Figure 7. It shows the potentiodynamic polarization curves of low carbon steel coated with a precursor sol of mixed Nb_xO_y/Al_2O_3 oxides. One can observe reproducibility of the results, since the potential and corrosion current densities (I_{corr}) did not vary significantly in the three test specimens analyzed (same synthesis conditions), showing evidence that the deposited layers exhibit homogeneous physical and chemical characteristics^{35,36}.

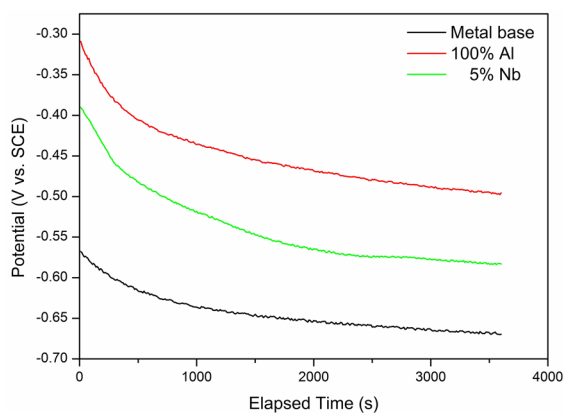


Figure 7. Open potential curves

This observation confirms the analysis of the EDXS spectra (Fig. 5a and Fig. 5b), which showed homogeneous distribution of Al and Nb atoms, since the segregation of phases of these compounds due to the thermal expansion coefficient gradient could produce faults in the deposited layers.

The aim of Figures 5 and 6 is to show the high degree of dispersion of Nb_xO_y in Al_2O_3 which is important to maintain the chemical and physical properties of the coating in oxide mixtures synthesized by sol-gel due to different rates of hydrolysis and condensation of aluminum alkoxides and niobium. In addition, it was not possible to estimate the thickness of the coating due to the nanometric characteristics of the film.

In the Nyquist diagram, Figure 8, the larger the semicircle described, the better the corrosion resistance of the sample, thus, the 100% Al film has presented the highest protection.

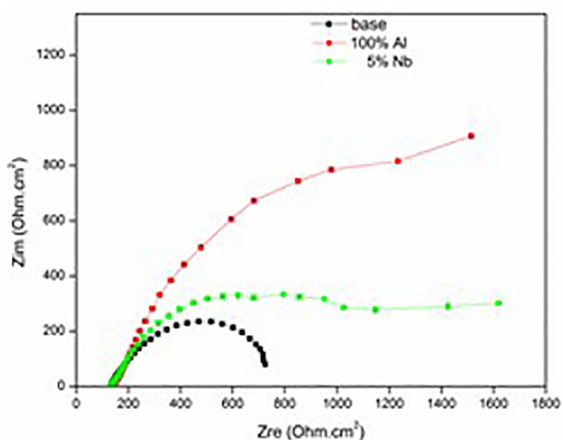


Figure 8. Nyquist representation

For comparison, Fig. 9 shows the polarization curves of the steel without coating and with surface coating of the precursor sol Nb_xO_y/Al_2O_3 and Al_2O_3 . Note that coatings improved the corrosion potential by about 0.2 V, indicating an improvement in anticorrosive properties. With both coatings used, the electric current decreased significantly when compared to the uncoated steel, showing independent behavior, since there is no intersection of the standard deviation under the three conditions of the test specimens. The open circuit time was 3600s.

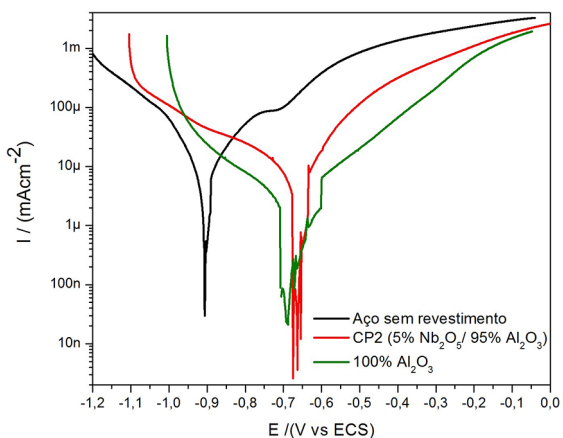


Figure 9. Polarization curves for AISI 1020, 3.5% NaCl, at room temperature: a) without coating; b) with the precursor sol coating of mixed Nb_xO_y/Al_2O_3 oxides with nominal values of 5% and 95%; c) with precursor sol coating of Al_2O_3

Additionally, the reduction of the average corrosion density of steel coated with sol precursor Al_2O_3 was about 50%, proving it was more effective in decreasing the corrosion process in the assayed conditions when compared to coated with precursor sol Nb_xO_y/Al_2O_3 .

However, the layers of Al_2O_3 on the metal substrate showed greater dispersion of the corrosion potential relative to the corrosion potential of the test samples coated with Nb_xO_y/Al_2O_3 . The effect of niobia seems to confer

greater physical homogeneity and coating chemistry, also indicating greater reproducibility in the process of these coatings, corroborating the above statements.

The higher current density of precursor sol coatings of Nb_xO_y/Al_2O_3 may be related to the appearance of cracking or a larger number of cracks in the deposited layer due to residual stress, or even the presence of electrical conductivity of the niobium oxides and the complexing effect of acetylacetone.

It is known that many oxide films have a variable oxidation state metal, being non-stoichiometric due to excess metal ions and oxygen ion deficiency³⁷. In the case of Nb ions, the compounds NbO, NbO₂ and Nb₂O₅ can be present in the deposited layer. Nb oxides have electrical properties that depend heavily on Nb's ion oxidation number³⁸. Nb₂O₅, the most stable niobium oxide, has excellent dielectric properties. However, NbO crystallized with a defective NaCl crystal structure has metallic behavior with high conductivity at room temperature. Additionally, NbO₂ with rutile structure is an n-type semiconductor with a small band gap of 0.5 eV at room temperature³⁸.

4. Conclusions

Aluminum oxide and mixed oxides of $Nb_xO_y/Al_{12}O_3$ were synthesized by the sol-gel method. Acetylacetone was used in mixed oxides as a complexing agent to control the hydrolysis and condensation rates of the aluminum isopropoxide and niobium pentaethoxide. Layers of these sols were deposited on AISI steel 1020 and the anticorrosive properties were investigated. Based on all the analyses, we can conclude that the presence of poorly crystallized boehmite alumina and mixed oxides of Nb_xO_y/Al_2O_3 was detected. Crystalline phases of Nb_xO_y were not observed.

The results obtained in EDXS analyses suggest that the rates of hydrolysis and condensation derived from sol-gel synthesis were controlled using acetylacetone, resulting in homogeneous distribution of the ions of Nb, Al, O and C.

The results of the potentiodynamic studies suggest that physical and chemical characteristics of the deposited layers are homogeneous, indicating the reproducibility of the deposition process and confirming the homogeneous characteristics of EDXS analysis.

The deposited layers of the precursor sol of both Nb_xO_y/Al_2O_3 and Al_2O_3 yielded improvements in anti-corrosion properties by increasing the potential for corrosion. The corrosion current of the coated samples decreased significantly compared to bare steel samples.

However, the coated steel showed different behavior with the two kinds of precursors, since the average current density of steel coated with the precursor sol Al_2O_3 was about 50% lower than the current density of the Nb_xO_y/Al_2O_3 precursor layers, being more efficient in the oxidation protection process. Moreover, the presence of niobium oxide seems to have provided greater homogeneity and

and better physicochemical properties of the coating, and hence better reproducibility of the process, since the steels coated with the precursor sol Nb_xO_y/Al_2O_3 showed less dispersion of the corrosion potential.

5. Acknowledgements

We are grateful for the financial support of FAPERJ, CAPES, CNPq and CENANO - INT.

6. References

1. Brinker CJ, Scherer GW. *Sol-Gel Science: The Physics and Chemistry of Sol-Gel Processing*. Boston: Academic Press; 1990.
2. Pierre AC. *Introduction to Sol-Gel Processing*. New York: Springer US; 1998.
3. Seok SI, Kim JH, Choi KH, Hwang YY. Preparation of corrosion protective coatings on galvanized iron from aqueous inorganic-organic hybrid sols by sol-gel method. *Surface and Coatings Technology*. 2006;200(11):3468-3472.
4. Carbajal-de la Torre G, Espinosa-Medina MA, Martínez-Villafañe A, González-Rodríguez JG, Castaño VM. Study of Ceramic and Hybrid Coatings Produced by the Sol-Gel Method for Corrosion Protection. *The Open Corrosion Journal*. 2009;2(1):197-203.
5. Checmanowski JG, Gluszek J, Masalski J. The effect of sequence of sol-gel multilayer coatings deposition on corrosion behaviour of stainless steel 316L. *Materials Science*. 2003;21(4):387-396.
6. Zhang X, Wu Y, Liu G, He S, Yang D. Investigation on sol-gel boehmite-AlOOH films on Kapton and their erosion resistance to atomic oxygen. *Thin Solid Films*. 2008;516(15):5020-5026.
7. Suwanboon S. The Properties of Nanostructured ZnO Thin Film via Sol Gel Coating. *Naresuan University Journal*. 2008;16(2):173-180.
8. Pepe P, Galliano P, Aparicio M, Durán A, Céré S. Sol-gel coatings on carbon steel: Electrochemical evaluation. *Surface and Coatings Technology*. 2006;200(11):3486-3491.
9. Ruhi G, Modi OP, Singh IB. Hot Corrosion Behavior of Sol-Gel Nano Structured Zirconia Coated 9Cr1Mo Ferritic Steel in Alkali Metal Chlorides and Sulphates Deposit Systems at High Temperatures. *Journal of Surface Engineered Materials and Advanced Technology*. 2013;3(1A):55-60.
10. Kamiya K. Sol-Gel Prepared Glass and Ceramic Fibers. In: Klein L, Aparicio A, Jitianu A, eds. *Handbook of Sol-Gel Science and Technology*. Chem: Springer; 2004.
11. Simões AZ, Zaghete MA, Stojanovic BD, Gonzalez AH, Riccardi CS, Cantoni M, et al. Influence of oxygen atmosphere on crystallization and properties of LiNbO₃ thin films. *Journal of the European Ceramic Society*. 2004;24(6):1607-1613.
12. Fang X, Yu Z, Sun X, Liu X, Qin F. Formation of superhydrophobic boehmite film on glass substrate by Sol-Gel method. *Frontiers of Chemical Engineering in China*. 2009;3(1):97-101.
13. Li H, Zhao G, Han G, Song B. Hydrophilicity and photocatalysis of Ti_{1-x}V_xO₂ films prepared by sol-gel method. *Surface and Coatings Technology*. 2007;201(18):7615-7618.

14. Çamurlu HS, Kesmez Ö, Burunkaya E, Kiraz N, Yesil Z, Asiltürk M, et al. Sol-gel thin films with anti-reflective and self-cleaning properties. *Chemical Papers*. 2012;66(5):461-471.
15. Dou Y, Cai S, Ye X, Xu G, Hu H, Ye X. Preparation of mesoporous hydroxyapatite films used as biomaterials via sol-gel technology. *Journal of Sol-Gel Science and Technology*. 2012;61(1):126-132.
16. Wan Y, Sun B, Liu W, Qi C. Tribological performance of fatty acid modification of sol-gel TiO₂ coating. *Journal of Sol-Gel Science and Technology*. 2012;61(3):558-564.
17. Tadanaga K. Preparation and application of alumina- and titania nanocrystals-dispersed thin films via sol-gel process with hot water treatment. *Journal of Sol-Gel Science and Technology*. 2006;40(2-3):281-285.
18. Rosero-Navarro NC, Pellice SA, Durán A, Aparicio M. Effects of Ce-containing sol-gel coatings reinforced with SiO₂ nanoparticles on the protection of AA2024. *Corrosion Science*. 2008;50(5):1283-1291.
19. Podchernyaeva IA, Lavrenko VA, Schvets VA, Frolov AA, Teplenko MA. Formation of a corrosion-resistant layer on steel by reaction with a Si₃N₄-Al₂O₃ composite under the conditions of light-thermal treatment. *Powder Metallurgy and Metal Ceramics*. 2001;40(1-2):44-48.
20. Shen GX, Chen YC, Lin CJ. Corrosion protection of 316 L stainless steel by a TiO₂ nanoparticle coating prepared by sol-gel method. *Thin Solid Films*. 2005;489(1-2):130-136.
21. Guglielmi M. Sol-Gel Coatings on Metals. *Journal of Sol-Gel Science and Technology*. 1997;8(1-3):443-449.
22. Abuín M, Serrano A, Llopis J, García MA, Carmona N. Silica doped with lanthanum sol-gel thin films for corrosion protection. *Thin Solid Films*. 2012;520(16):5267-5271.
23. Graham RA, Sutherland RC, Chang W. Niobium and niobium alloys in corrosive applications. In: *Niobium Science and Technology. Proceedings of International Symposium Niobium*; 2001 Dec 2-5; Orlando, FL, USA. p. 337-355.
24. Masalski J, Gluszek J, Zabrzanski J, Nitsch K, Gluszek P. Improvement in corrosion resistance of the 316L stainless steel by means of Al₂O₃ coatings deposited by the sol-gel method. *Thin Solid Films*. 1999;349(1-2):186-190.
25. Ruhi G, Modi OP, Sinha ASK, Singh IB. Effect of sintering temperatures on corrosion and wear properties of sol-gel alumina coatings on surface pre-treated mild steel. *Corrosion Science*. 2008;50(3):639-649.
26. Ruhi G, Modi OP, Jha AK, Singh IB. Characterization of corrosion resistance properties of sol-gel alumina coating in mine water environment. *Indian Journal of Chemical Technology*. 2009;16:216-220.
27. Zhou M, Yang Q, Troczynski T. Effect of substrate surface modification on alumina composite sol-gel coatings. *Surface and Coatings Technology*. 2006;200(8):2800-2804.
28. Santos PS, Coelho ACV, Santos HS, Kiyohara PK. Preparation of pseudoboehmite aqueous sols with fibrils of different lengths. *Cerâmica*. 2009;55(334):135-144.
29. Tettenhorst R, Hofmann DA. Crystal chemistry of boehmite. *Clays and Clay Minerals*. 1980;28(5):373-380.
30. Zhou RS, Snyder RL. Structures and transformation mechanisms of the η, γ and θ transition aluminas. *Acta Crystallographica Section B*. 1991;47(Pt 5):617-630.
31. Munhoz AH Jr, de Miranda LF, Uehara GN. Study of pseudoboehmite synthesis by sol-gel process. *Advances in Science and Technology*. 2000;45:260-265.
32. Munhoz AH Jr, de Paiva H, de Miranda LF, de Oliveira EC, Andrades RC, Cabral A Neto. Synthesis and Characterization of Pseudoboehmite and Gamma-Alumina. *Materials Science Forum*. 2015;820:131-136.
33. Ahenach J, Cool P, Impens REN, Vansant EF. Silica-Pillared Clay Derivatives Using Aminopropyltriethoxysilane. *Journal of Porous Materials*. 2000;7(4):475-481.
34. Uekawa N, Kudo T, Mori F, Wu YJ, Kakegawa K. Low-temperature synthesis of niobium oxide nanoparticles from peroxo niobic acid sol. *Journal of Colloid and Interface Science*. 2003;264(2):378-384.
35. Zhao JP, Liu XR, Qiang LS. Characteristics of the precursors and their thermal decomposition during the preparation of LiNbO₃ thin films by the Pechini method. *Thin Solid Films*. 2006;515(4):1455-1460.
36. Bouquet V, Longo E, Leite ER, Varela JA. Influence of heat treatment on LiNbO₃ thin films prepared on Si(111) by the polymeric precursor method. *Journal of Materials Research*. 1999;14(7):3115-3121.
37. Sikula J, Hlavka J, Sedlakova V, Grmela L. *Conductivity Mechanisms and Breakdown Characteristics of Niobium Oxide Capacitors*. Fountain Inn: A VX Corporation; 2003.
38. Lee S, Yoon H, Yoon I, Kim S. Single Crystalline NbO₂ Nanowire Synthesis by Chemical Vapor Transport Method. *Bulletin of Korean Chemical Society*. 2012;33(3):839-842.